ELSEVIER

Materials Science and Engineering A 390 (2005) 334–343

MATERIALS SCIENCE & ENGINEERING A

www.elsevier.com/locate/msea

Strain rate sensitivity of the commercial aluminum alloy AA5182-O

R.C. Picu[a,*], G. Vincze[b], F. Ozturk[a], J.J. Gracio[b], F. Barlat[b,c], A.M. Maniatty[a]

[a] *Department of Mechanical, Aerospace and Nuclear Engineering, Rensselaer Polytechnic Institute, Troy, NY 12180, USA*
[b] *Center for Mechanical Technology and Automation, University of Aveiro, 3810-193 Aveiro, Portugal*
[c] *Alcoa Technical Center, Alcoa Center, PA 15069, USA*

Received 8 January 2004; received in revised form 5 August 2004

Abstract

The mechanical behavior of the commercial aluminum alloy AA5182-O is investigated at temperatures ranging from −120 to 150 °C and strain rates from 10^{-6} to 10^{-1} s^{-1}. The strain rate sensitivity parameter is determined as a function of temperature and plastic strain, and the strain rate and temperature range in which dynamic strain aging leads to negative strain rate sensitivity is mapped. The effect of dynamic strain aging on ductility and strain hardening is investigated. The sensitivity of the measured quantities to the experimental method employed and their dependence on grain shape are discussed. The experimental data are compared with the predictions of a model constructed based on a recently proposed mechanism for dynamic strain ageing. The mechanism is based on the effect solute clustering at forest dislocations has on the strength of dislocation junctions. The model is shown to reproduce qualitatively the experimental trends.

Keywords: Strain rate sensitivity; Dynamic strain ageing; Portevin–LeChatelier effect; Al alloys

1. Introduction

Aluminum alloys are important technological materials primarily due to their advantageous strength to weight ratio. They are used in diverse applications ranging from packaging to the aeronautic industry. Current alloy design is primarily aimed at improving material properties in order to access new markets. An important example is automobile body panels. This would significantly reduce automobile weight, which translates into fuel savings and associated environmental advantages.

Important candidates for such applications are the alloys from the 5000 class whose primary alloying element is Mg. These alloys are currently used extensively in beverage packaging and other applications. They may be drawn in thin sheets and offer significant strength. However, their deformation at room temperature is discontinuous, with the strain localizing in narrow bands that leave undesirable traces on the surface of the final product. This is the signature of the Portevin–LeChatelier phenomenon (PLC), which manifests itself in certain ranges of temperature and strain rate.

The repeated strain localization is due to the negative strain rate sensitivity (SRS) of the material which, in turn, is caused by smaller scale phenomena associated with interactions between solute and dislocations, referred to as dynamic strain aging (DSA). Hence, PLC is one of the macroscopic manifestations of DSA.

Both PLC and DSA were extensively studied over the last several decades [1–4] with the goal being to achieve a better understanding of the small-scale processes and of the multiscale mechanisms that link the nanoscale DSA to the macroscale PLC effect. The technological goal is to increase the SRS to positive values in the range of temperatures and strain rates relevant for industrial processes. This would insure material stability during processing and would eliminate PLC. In particular, in Al–Mg alloys it is desired to increase the SRS parameter and to eliminate the PLC effect at room temperature.

Serrated flow was observed in many dilute solid solutions having f.c.c. (Al, Cu and Ni–based alloys), b.c.c. (e.g. in steels) and h.c.p. lattices (Zn-based alloys). The phenomenon

* Corresponding author. Tel.: +1 518 2762195; fax: +1 518 2766025.
E-mail address: picuc@rpi.edu (R.C. Picu).

0921-5093/$ – see front matter © 2004 Elsevier B.V. All rights reserved.
doi:10.1016/j.msea.2004.08.029

was even observed in commercially pure Al, due to traces of impurities [5].

Al–Mg alloys are some of the most studied systems in connection with negative SRS. Binary Al–Mg [6–8] as well as the equivalent commercial alloys [9–13] received attention. Reviews of the current experimental state of the art are given in Refs. [14,15]. A significant amount of data exists on the effect of Mg, the contribution of the other solute species, the role of precipitates and that of grain boundaries, the dependence on grain size, as well as on macroscopic parameters such as the specimen geometry and state of stress and strain.

The microscopic mechanism leading to negative SRS is still a matter of debate. Mobile solute atoms tend to cluster at dislocations driven by their primarily elastic interaction with the strain field generated by these defects. Clustering leads to an enhancement of the apparent lattice resistance to dislocation motion. In the current physical picture of DSA it is considered that, if the solute has sufficient mobility, clustering may occur during the relatively short time a mobile dislocation is arrested at obstacles such as forest dislocations, precipitates and grain boundaries [2,16]. Clustering is assumed to occur either by lattice diffusion, from the lattice to the arrested mobile dislocation, or by pipe diffusion, from the solute cluster on the forest dislocation, along the core of the mobile dislocation.

At high strain rates, when the average arrest time is short, the clusters are too small to produce an effective enhancement of the strength of the obstacle and the PLC effect is not observed. Clustering contributes to the intrinsically unsteady motion of dislocations in that a higher resolved shear stress is needed to break free the defect from the cloud, while a relatively low stress is required to keep it moving after this event. This process leads to negative strain rate sensitivity and strain localization. The temperature is important since it controls solute mobility and clustering rate.

This physical picture was recently challenged by a series of atomistic simulations of Mg diffusion along the core of various dislocations in Al [17]. It was shown that pipe diffusion, as well as bulk diffusion, must be assisted by vacancies in order to occur at reasonable rates at room temperature. However, it is now accepted that vacancies do not play a central role in DSA [18]. They certainly favor the effect (enhance diffusion), but the DSA mechanism must be independent of their presence and concentration. Notwithstanding the effect of vacancies, pipe diffusion appears to be as slow as bulk diffusion in this material system and at room temperature. In turn, this implies that clustering of mobile dislocations during their arrest time at obstacles, t_w, either by bulk or pipe diffusion, is too slow for the mechanism to explain the macroscopic phenomenon.

A new mechanism, which does not require that solute clusters form on mobile dislocations during t_w, was recently proposed [19]. The mechanism is based on a mesoscopic analysis of the interaction of a mobile, unclustered dislocation with a clustered forest. It is shown that the strength of dislocation junctions (which control the athermal component of the flow stress) is strongly affected by the presence of clusters on forest dislocations. Hence, the average strength of junctions depends on the average size of clusters on forest dislocations which, in turn, depends on the residence time of forests, t_a. At given plastic strain, the residence time of forests is a function of the strain rate. Increasing the deformation rate reduces the ageing time of forests, which leads to smaller clusters and lower dislocation junction strength, i.e. negative SRS.

In this report, we provide new data on the mechanical behavior of one of the most important commercial alloys from this series: AA5182-O. The attention is focused here on mapping the domain of negative strain rate sensitivity and on determining the effect of temperature on ductility in conjunction with the negative SRS, for the as-received material. We also investigate the variation with temperature of the strength and the effect of the grain shape on the rate sensitivity of the material. The experimental data are compared with predictions of the model proposed in Ref. [19].

2. The material

The material used in this study is supplied by Alcoa in the form of rolled and annealed sheet of 1 mm thickness. It is primarily a solid solution of 4.5 wt.% Mg in Al, with other alloying elements being Mn (0.2–0.5%), Cr (0.1%), Cu (0.15%), Zn (0.25%), Si (0.2%), Ti (0.1%) and Fe (0.35%).

Mg is added for strength and is frozen in solid solution at room temperature. Mg forms a coherent beta prime phase with Al, which is present as a fine dispersion at temperatures below 200 °C. This phase is relatively stable and has a slow unbinding kinetics. However, the thermodynamically stable phase is Al_3Mg_2, which precipitates only upon significant annealing at temperatures immediately below 200 °C. The mechanical properties of the material at room temperature are controlled by the Mg atoms in solid solution [15].

Cr and Mn are added as grain growth stabilizers. As reported in Refs. [20–22] Cr, Fe and Mn form $(Mn,Fe)Al_6$, $Cr_2Mg_3Al_{18}$ and $FeCrAl_3$ precipitates, while Si forms silicides (Mg_2Si). Some of these are located along grain boundaries and are assumed to contribute little to the negative SRS and PLC. However, they may lead to cavitation during hot forming operations. Other precipitates are located within the grains. Copper adds to strength and also stabilizes the precipitates at high temperature [22].

The material was annealed after the repeated rolling operations and, in the as-received state, exhibits grain shape anisotropy. The grain size is 50 and 15 μm along and perpendicular to the rolling direction, respectively. The crystallographic texture was characterized using X-ray diffraction with the texture measurement instrument (TMI) [23]. In this technique, a high energy beam crosses the entire specimen, giving the average texture throughout the entire thickness of the sheet. The (1 1 1), (2 0 0) and (2 2 0) pole figures were measured and used to calculate the orientation distribution function. The crystallographic texture was rather weak and

the corresponding range of Taylor factor in uniaxial tension over the different directions of the sheet was between 3.02 and 3.06. Standard mechanical test results conducted a 0°, 45° and 90° from the rolling direction led to yield stresses of 141, 135 and 138 MPa in these respective directions. The measured r values (width to thickness strain ratio) were 1.0, 1.2 and 1.0, respectively.

3. Experimental procedure

Uniaxial tension tests were carried out using ASTM tension specimens with 10 mm gauge width. Most specimens were cut with their axis aligned with the rolling direction. The rolling direction was aligned perpendicular to the loading direction in several specimens in order to investigate its effect on the strain rate sensitivity of the material. The material was tested in the as-received conditions, with no heat treatment being performed.

The strain rate sensitivity was measured in constant strain rate tests as well as in strain rate jump tests. A strain rate differential of 1:100 was used in most cases. In the strain rate jump tests the rate was changed by one or two orders of magnitude in separate tests and both the instantaneous and the steady state rate sensitivity were measured. The base rate was $10^{-4}\,s^{-1}$.

Tests were performed at non-ambient temperature in air. The temperature was measured with a thermocouple on the surface of the specimen and was kept constant to within ±0.5 °C.

4. Results

The experimental data are presented in this section. We focus on mapping the rate–temperature domain of negative SRS and on the variation of the ductility and strength with temperature. Other observations pertaining to the manifestation of the PLC effect are mentioned in passing.

4.1. The strain rate sensitivity parameter

Tests were performed at temperatures between −120 and 150 °C and at strain rates ranging from 10^{-6} to $10^{-1}\,s^{-1}$. Typical stress–strain curves are shown in Fig. 1 as obtained at $T = -100$ °C, room temperature and at $T = +100$ °C. Serrated flow, which is indicative of negative SRS, was observed in all tests performed at temperatures in the range −80 to 100 °C.

The strain rate sensitivity parameter, m, was computed using the equation:

$$m = \frac{\log[\sigma_1/\sigma_2]}{\log[\dot{\varepsilon}_1/\dot{\varepsilon}_2]} \quad (1)$$

For m evaluated from constant strain rate tests, σ_1 and σ_2 represent the flow stress at the current strain, measured in tests performed with strain rates $\dot{\varepsilon}_1$ and $\dot{\varepsilon}_2$, respectively.

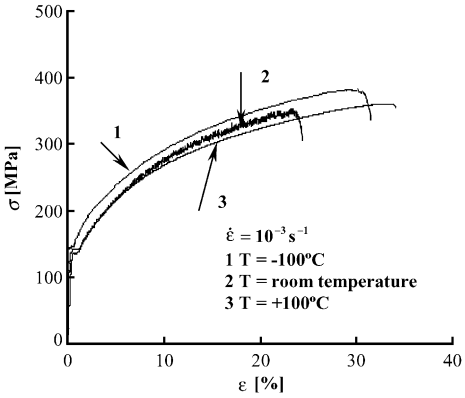

Fig. 1. Typical true stress–true strain curves at three temperatures within and outside the PLC range. The curves are serrated within the domain in which the SRS is negative and smooth outside. The ductility is reduced within the domain.

In strain rate jump tests, two types of strain rate sensitivity may be defined [24]. The instantaneous rate sensitivity, m_i, is computed from the instantaneous variation of the stress associated with a strain rate jump from $\dot{\varepsilon}_1$ to $\dot{\varepsilon}_2$. The steady-state strain rate sensitivity, m, is computed based on the $\Delta\sigma$ determined by extrapolating the flow curve after the transient following the strain rate jump, to the moment of the jump. The steady state rate sensitivity may be expressed as the sum of the instantaneous measure and that corresponding to a transient, m_t: $m = m_i + m_t$. The instantaneous measure is always positive and increases with strain [25]. In solid solutions with mobile solutes, m_t is negative. When the steady state rate sensitivity becomes negative ($m_i < |m_t|$), conditions exist for the loss of stability of the material and appearance of the PLC effect.

The variation of m with strain is shown in Fig. 2 for three temperatures. The strain rate sensitivity is negative for all strains at room temperature and 50 °C. At 110 °C, m is

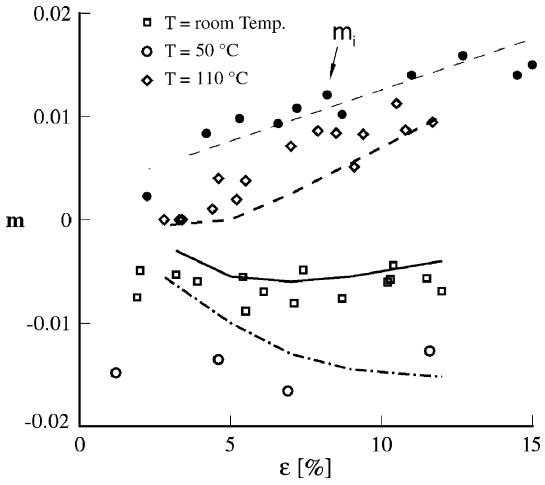

Fig. 2. Variation of the strain rate sensitivity parameter m with strain at three temperatures within the negative SRS range. The open data points are obtained from strain rate jump tests, while the curves correspond to constant strain rate experiments. The filled symbols correspond to the instantaneous rate sensitivity, m_i, and the dashed straight line is a fit to the data.

negative at small plastic strains and becomes positive as deformation proceeds. At all other temperatures within the PLC range, m initially decreases slightly and then remains essentially constant with ε. Since m decreases with strain, the strain rate sensitivity of the flow stress is more pronounced than that of the yield stress.

The open data points are obtained from strain rate jump tests (strain rate differential 1:100, base rate $10^{-4}\,s^{-1}$), while the lines represent results obtained from constant strain rate tests (same strain rate differential and base rate). Reasonable agreement is seen between the two sets of data. Furthermore, m computed in strain rate jump tests from a jump up in strain rate is in good agreement with the same quantity computed from a jump down in rate at the same strain. The pros and cons of the two types of tests were discussed in Ref. [26]. The strain rate jump tests are assumed to provide more reliable data since the rate sensitivity is measured in a given specimen at given strain and therefore at given internal material state. When m is evaluated from constant strain rate tests, two different specimens subjected to different deformation histories are used. Hence, if the deformation history is important at the respective test temperature, the results are expected to differ.

The instantaneous rate sensitivity parameter provides information on the response to a strain rate change of the current material structure. This quantity is important in that a larger (positive) value promotes homogeneous plastic deformation, as discussed above. This measure is shown in Fig. 2 (filled symbols and dashed line). m_i is seen to increase with strain as observed in other material systems [25]. The variation is linear in the considered range of strains, the equation of the straight line in Fig. 2 being $m_i = 0.0023 + 0.00106\varepsilon$. Hence, the extrapolated value of m_i at zero strain is 0.0023. The curves corresponding to m measured from constant rate tests seem to converge at zero strain to a value close to the above. Hence, the transient component of the rate sensitivity, m_t, starts from zero and decreases significantly with strain, which suggests that the negative SRS is associated with phenomena that occur during the deformation process, rather than to the material condition before deformation. This measurement of m_i is made at $T = 100\,^{\circ}C$. However, it is known that m_i is essentially temperature independent at all strains [25].

The variation with temperature of the strain rate sensitivity parameter m is discussed next. Fig. 3 shows m evaluated from constant rate tests for temperatures between −120 and 150 °C. The data correspond to a strain rate differential of 1:100 and to base rate of $\dot{\varepsilon}_1 = 10^{-3}\,s^{-1}$, and are collected at plastic strains of 10 and 20%. The range of negative rate sensitivity is −80 to 110 °C. This is in agreement with Ref. [27] in which m was found to be negative in a binary Al–Mg alloy tested at rates between 10^{-6} and $10^{-2}\,s^{-1}$ between −80 and 80 °C. This supports the conclusion that the mechanical behavior of the commercial alloy is essentially determined by the Mg solute. It is noted in passing that m is essentially independent of the rolling reduction of the material [35] and the strain rate sensitivity measured here is expected to be valid for this material even when processed to other reductions.

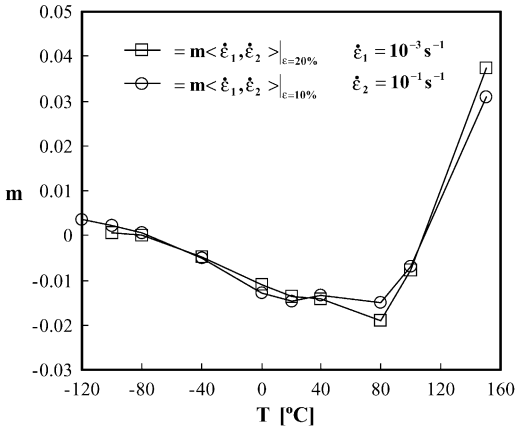

Fig. 3. Variation of the steady-state strain rate sensitivity parameter m with temperature.

At temperatures above 120 °C, m depends on the strain rate differential and the plastic strain at which the readings are made (see also Fig. 2). In this range of temperatures for which $m > 0$, m increases with plastic strain. On the contrary, in the low temperature range −80 to −120 °C ($m > 0$), the parameter slightly decreases with the plastic strain.

The variation of m with temperature suggests that the activation energy for PLC at the low and the high temperature ends of the PLC range is different. The transition from positive to negative m is very gradual at $T \sim -100\,^{\circ}C$, while at $T \sim 100\,^{\circ}C$ it is quite abrupt. This suggests that different DSA mechanisms dominate the behavior in different temperature ranges. Ling and McCormick [25] observed that the high temperature behavior does not appear to be due to structural changes such as precipitation, which could change the nature of the rate controlling obstacles to dislocation motion. Rather, the diffusion-controlled kinetics of DSA appears to be different at high and low temperatures. This phenomenon was recently analyzed in detail by Nortmann and Schwink [28,29] and by Hahner [30]. They concluded that several types of pipe diffusion (along the core of the partials, along the stacking fault ribbon, etc.) might become active at high temperature. However, as discussed in Section 1, the effectiveness of pipe diffusion as the dominant mechanism for DSA is questioned [17]. In the mechanism proposed in Ref. [19], the two activation energies are associated with bulk diffusion and with the dissolution at high temperatures of clusters formed on forest dislocations. This second quantity is determined by the binding energy of Mg atoms to dislocation cores. The discussion of this issue is deferred to Section 5.

The PLC domain (considered approximately identical with the negative SRS domain) was mapped and is shown in Fig. 4 in the $\log(\dot{\varepsilon}) - 1/T$ plane. Open/filled symbols represent conditions in which PLC is not/is observed. The data points well-within the domain are not shown, for clarity. Data presented for the same commercial alloy by Abbadi et al. [31]

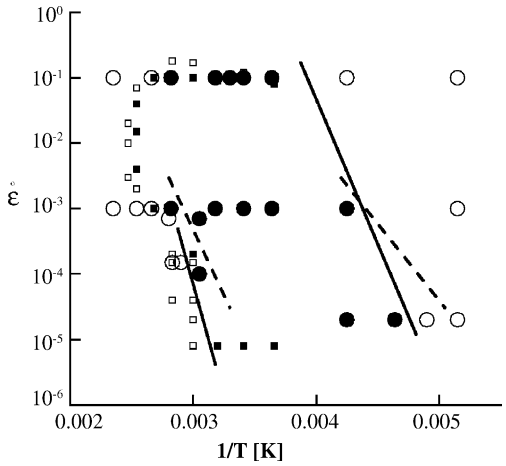

Fig. 4. Map of the PLC domain in the $\log(\dot{\varepsilon}) - (1/T)$ plane. The open/filled symbols correspond to conditions in which the PLC effect is not/is observed. The smaller symbols are reproduced from Ref. [31], while the two dashed lines are the boundaries of the PLC domain reported in Ref. [32]. The continuous lines are the boundaries of the PLC domain fitted to the current data.

and by Pink and Grinberg [32] (corresponding to a similar alloy with 5% Mg) are included in the figure. The data from Ref. [31] are shown with smaller symbols, while only the two boundaries of the PLC domain from Ref. [32] are included. The three sets of data are in good agreement. Here we extend the domain investigated compared to the results presented in [31] by including the low temperature boundary of the PLC region. The domain is bounded at high strain rates by an almost horizontal line at $\dot{\varepsilon} = 10^{-1}\,\mathrm{s}^{-1}$. The high and low temperature boundaries are essentially straight parallel lines (within the current accuracy). The slopes of these lines correspond to activation energies of 1.09 and 0.86 eV, for the high and low temperature boundaries, respectively. The slopes of the respective boundaries from Ref. [32] are 0.8 and 0.46 eV, respectively. The data from Ref. [31] indicate the existence of a kink in the high temperature boundary at $T \sim 60\,^{\circ}\mathrm{C}$ and strain rate $5 \times 10^{-4}\,\mathrm{s}^{-1}$, which required the fitting of the high temperature boundary to our data to be made at small strain rates only. The domain is also bounded at high temperatures and higher strain rates.

The effect of grain shape anisotropy on the measured strain rate sensitivity parameter was evaluated at room temperature. Specimens in which the loading direction was aligned with the rolling direction, and samples in which the two directions are perpendicular were subjected to strain rate jump tests. Within the scatter of the data, *m* does not appear to be sensitive to orientation (Fig. 5).

4.2. Observations of serrated flow

The macroscopic observation of serrated flow is an indication of the negative SRS. The serrations observed in polycrystalline materials in which solute is substitutional are quite regular and have been previously classified into three major

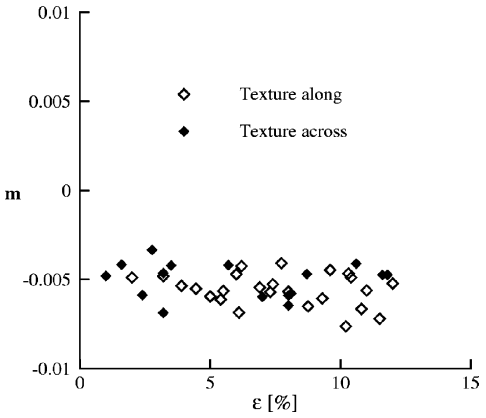

Fig. 5. Strain rate sensitivity parameter *m* measured at room temperature in specimens in which the loading direction is normal (closed symbols) and aligned (open symbols) to the rolling direction.

groups denoted by A–C. At room temperature and at strain rates below $10^{-4}\,\mathrm{s}^{-1}$ we observe type C serrations, in which the stress drops below the undisturbed stress–strain curve [33]. As the rate increases, the nature of the serrated flow changes, with a mixture of types A and B serrations being observed. No such specific observations were made at other temperatures. This observation is in agreement with the data of Kral and Lukac [34] who tested an Al–4.8% Mg alloy at room temperature and several strain rates, and those of Romhanji et al. [35] who report type C serrations at room temperature and strain rates below $10^{-3}\,\mathrm{s}^{-1}$ in a similar alloy. This last group observes type A + B serrations at a rate of $6.7 \times 10^{-3}\,\mathrm{s}^{-1}$, while at $6.7 \times 10^{-2}\,\mathrm{s}^{-1}$ a succession of plateaus of serrations is observed.

It is noted that occasionally "traveling bands" (type B, in the terminology used in Ref. [36]) appear at room temperature and low strain rates ($10^{-4}\,\mathrm{s}^{-1}$). Fig. 6 shows such an example in which regions denoted by *P* correspond to the intermittent propagation of a localization band along the gauge

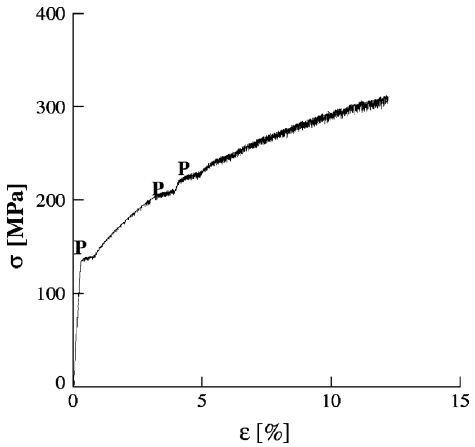

Fig. 6. Stress–strain curve exhibiting the yield point phenomenon and two plateaus corresponding to the propagation of "traveling bands" (*P*). Serrations are observed from the yield point up to specimen failure. The test was performed at room temperature and with a strain rate of $10^{-3}\,\mathrm{s}^{-1}$.

of the specimen. Outside of these plateaus the serrations are random. This was observed in several specimens only and could not be related to specifics of the specimen microstructure or geometry.

Each serration corresponds to the formation of a localization band on the surface of the specimen. The bands run at an angle of 63° ± 2° with respect to the loading direction, in agreement with the value of 61° reported by Chihab et al. [36] for an Al–5 at.% Mg alloy. It was shown that the angle depends on texture and is expected to range from 52° to 66° as a function of the orientation of the load axis with respect to the rolling direction [37]. The continuum analysis of localization in the direction of no extension for an isotropic sheet subjected to uniaxial loading predicts the angle to be 54.74° [38]. However, if the magnitude of the strain in the width direction is less than that in the thickness direction due to material constraints, the angle is predicted to be larger, with the extreme being 90° for the case of plane strain, i.e. zero strain across the width of the specimen. Li and Lege [13] discuss the effect of the macroscopic stress and strain state on the appearance of serrated flow and surface markings.

Discontinuous yielding and initial Lüdering is observed in all specimens loaded at rates below $10^{-2}\,s^{-1}$. Such yield points phenomena are not observed during transients following strain rate jumps in tests performed under the same conditions. Mulford and Kocks [2] observe something that looks like discontinuous yielding during strain rate jumps in Inconel 600 only if the flow is smooth. Jumps performed during jerky flow were not found to exhibit a yield point phenomenon.

As discussed by Romhanji et al. [35] the yield point phenomenon is observed only in pre-deformed specimens with high dislocation density that were rolled to reductions larger than 20%. This is also the case with the present specimens. Ohtani and Inagaki [39] similarly observe that Al–4.4% Mg specimens cooled in the furnace from a heat treatment temperature of 450 °C always exhibit the yield point phenomenon and serrated flow from the very beginning of plastic deformation over a wide range of strain rates. They conjecture that actually Lüdering induces the PLC effect in the region just behind the Lüders band front, a phenomenon not observed in this study.

No critical strain for the onset of PLC, ε_c, is observed in all tests performed at rates between 10^{-5} and $10^{-2}\,s^{-1}$ (e.g. Fig. 6). The serrated flow begins immediately after yielding and continues with increasing magnitude up to specimen failure. Close to the upper strain rate limit of the negative SRS domain in Fig. 4, we observe a temperature-dependent critical strain that has a minimum of 3.5% at 40 °C.

The absence of a critical strain was reported by Romhanji et al. [35] for an Al–6.5% Mg alloy tested at room temperature and at rates between 6.7×10^{-4} and $6.7 \times 10^{-2}\,s^{-1}$. They observe this behavior in all rolled specimens, the critical strain increasing upon annealing. Balik and Lukac [6] and Kral et al. [40] also report essentially no critical strain for rates between 10^{-4} and $10^{-2}\,s^{-1}$ in Al–3% Mg and Al–4.8% Mg, respectively. However, they see a net ε_c at room temperature and rates below 5×10^{-5} and above $10^{-2}\,s^{-1}$. Abbadi et al. [31] report temperature and strain rate-dependent critical strains for their material.

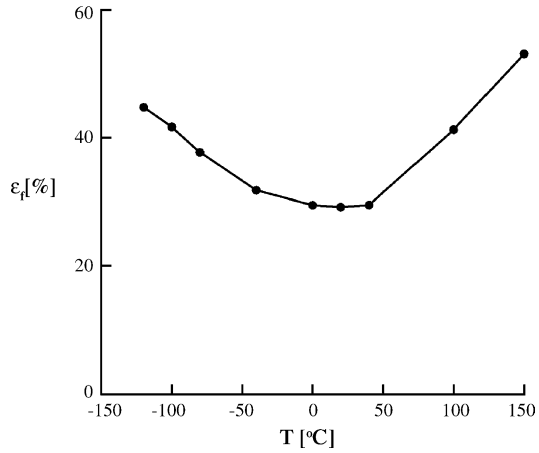

Fig. 7. Variation of the total elongation at failure with temperature.

4.3. Ductility and strength

In spite of their negative strain rate sensitivity, but because of their high rate of hardening, the Al–Mg alloys are some of the most ductile Al alloys currently in use. This makes them useful in a variety of applications in which forming with large reduction ratios are required. Therefore, it is interesting to determine to what extent the ductility of the commercial alloy is affected by DSA.

Fig. 7 shows the total elongation at failure measured in tests performed at $10^{-3}\,s^{-1}$ and at various temperatures within and outside of the negative SRS domain (Fig. 4). As the temperature increases from −120 °C, the ductility decreases continuously while DSA becomes more pronounced, reaches a minimum at room temperature and then increases upon further increasing the temperature. This behavior may also be observed in Fig. 1. The fact that minimum ductility is obtained at room temperature, which is typically the desired processing temperature, is detrimental and is an incentive for material development. The ductility follows the same trend as the strain rate sensitivity with lower ductility at temperatures corresponding to lower strain rate sensitivities. Skinner et al. [41] make a similar observation, but at higher temperatures in tests on round specimens of Al–Fe–V–Si alloys.

It is noted that the variation of this measure of ductility with temperature correlates with the variation of the transient (and therefore the steady state) strain rate sensitivity parameter, which is a direct indication that the reduction in ductility is due to the DSA.

The variation of the yield stress with temperature measured at a strain rate of $10^{-3}\,s^{-1}$ is shown in Fig. 8. As expected, DSA leads to an increase of the yield stress (relative to the generally decreasing trend of the yield stress versus temperature curve) in the range of temperatures in which its effect is macroscopically visible [11]. The observation

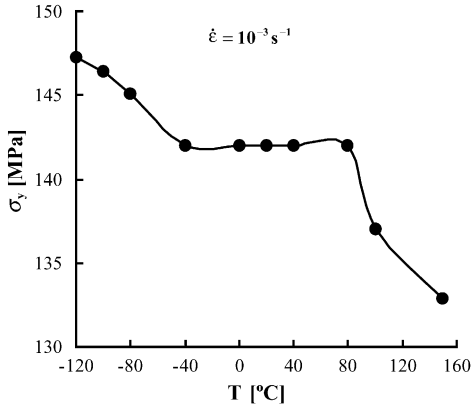

Fig. 8. Variation of the yield stress with temperature measured at $\dot{\varepsilon} = 10^{-3}\,s^{-1}$.

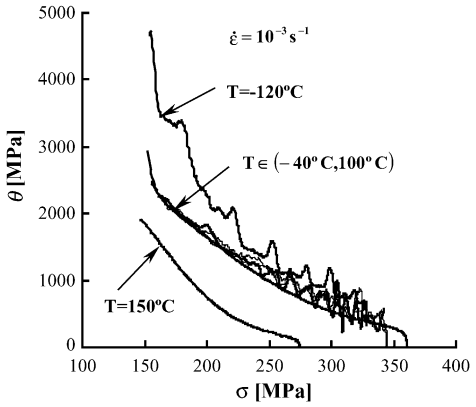

Fig. 9. Strain hardening vs. flow stress curve for several temperatures within and outside the PLC range.

remains valid for all flow stresses, which is supported by the data in Fig. 9.

Fig. 9 shows the strain hardening rate $\theta = d\sigma/d\varepsilon$ as a function of the flow stress for all temperatures considered in this study. The data were obtained from tests performed with strain rate $10^{-3}\,s^{-1}$. In the PLC range strain hardening is essentially independent of temperature. Normal behavior (continuously decreasing strain hardening rate at given flow stress, with temperature) is seen outside of the PLC range. It was suggested [42] that DSA enhances strain hardening through reducing dynamic recovery. An alternate explanation is proposed in the next section.

5. Comparison with model predictions

The experimental data are discussed in this section in conjunction with the DSA model presented in Ref. [19]. The model is briefly reviewed here.

As discussed in Section 1, it is currently accepted that, in general, DSA is due to the interaction of mobile solute atoms and dislocations. The solute and dislocations form a dynamic system in which solute diffuses to dislocations and dislocations move under stress. Mg diffusion in Al at room temperature and in absence of an excess of vacancies (at the thermodynamically stable vacancy concentration) was shown to be too slow to produce significant clustering at mobile dislocations during their arrest time at forest obstacles (t_w = 0.1–10 s, depending on strain rate). However, clustering at forest dislocations is assumed to be possible due to the relatively long residence time of these dislocations. The size of the cluster at a forest depends on its ageing time, t_a, and on temperature. The ageing time, in turn, depends on the rate of forest dislocation production or the imposed strain rate. At any given strain, the forest population contains dislocations on different clustering stages, depending on when they were produced.

The key insight on which the model is based is related to the strength of a junction formed by a mobile unclustered dislocation with a clustered forest. The analysis was performed with an orientation-dependent line tension model for the two dislocations [19]. The cluster is captured in the model as a binding energy per unit length of the forest dislocation (Q) to its initial position, occupied before the formation of the junction with the mobile dislocation. The binding energy is a function of the ageing time, t_a and temperature, T. It was shown that the strength of a typical junction (the Lomer–Cottrell lock) increases as Q increases from zero, and then reaches a Q-independent plateau. The variation is associated with a change in the dominant failure mode of the junction, from unzipping to the instability of one of the mobile dislocation branches. When Q is larger than a threshold value, the stair rod does not form and the two dislocations remain in the "crossed state". This configuration fails by the mobile dislocation instability and the strength is Q-independent. This behavior remains qualitatively similar for all loading paths (combinations of resolved shear stress applied to the forest and mobile dislocations).

Hence, at high strain rates the average cluster is small and the average junction strength is low. The situation is opposite at low strain rates, which leads to negative strain rate sensitivity.

The insight obtained from this analysis was captured in a model of the athermal component of the flow stress. The flow stress was evaluated by averaging over the strength of the whole population of junctions formed at given time/strain by a mobile dislocation and many forests of various cluster size. The averaging was performed using the method proposed by Hanson and Morris [43]. One of the main limitations of the treatment is that the fundamental information regarding the junction strength is obtained from the analysis of a single type of junction, the Lomer–Cottrell lock. Therefore, a quantitative comparison with experimental data is not possible and only overall trends may be evidenced.

The key parameter in the model is $\varepsilon_0 = \dot{\varepsilon} t_0$, where $\dot{\varepsilon}$ is the imposed strain rate and t_0 is the time constant of the clustering process at forest dislocations. t_0 is associated with bulk diffusion of solute. This parameter lumps the effects of strain rate

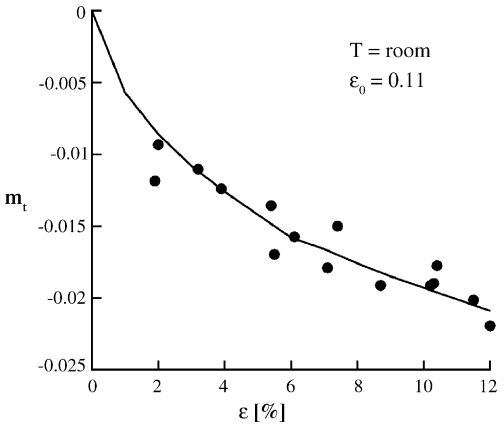

Fig. 10. Model prediction (line) and experimental data (points) for the variation of the transient component of m, m_t, with strain at room temperature. The data correspond to those in Fig. 2. The model prediction is evaluated by assuming $Q_s/A = 0.018$ [19], where A is the energy per unit length of an edge dislocation in Al.

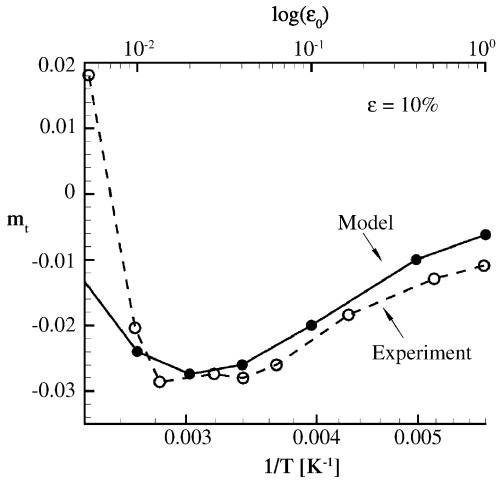

Fig. 11. Model prediction (continuous line and filled symbols) and experimental data (dashed line and open symbols) for the variation of the transient component of m, m_t, with $1/T$ at 10% strain. The data correspond to those in Fig. 3. The model prediction is evaluated by assuming $Q_s/A = 0.018$ [19], where A is the energy per unit length of an edge dislocation in Al.

and temperature, increasing linearly with strain rate and decreasing with increasing temperature. This is consistent with suggestions made in the literature [24] according to which the strain rate and the temperature may be combined into a single constitutive parameter of the form $\dot{\varepsilon}\ \exp[E/kT]$, where E is the activation energy for DSA. It is noted that an additional temperature dependence is included in Q, which is expected to decrease with increasing temperature due to the dissolution of clusters at high T [44].

The steady state SRS parameter results as the sum of two quantities, corresponding to the thermal and the athermal components of the flow stress. The thermal component of SRS is related to the interaction of dislocations with obstacles that may be overcome by thermal activation, and it is considered to be positive. The athermal component is associated with the formation of dislocation junctions and is affected by DSA, therefore being either positive or negative.

First, we compare the model predictions with the experimental values of m versus strain. Fig. 10 shows the transient SRS parameter computed from the data in Fig. 2, at room temperature. The test was performed with a base strain rate of $10^{-4}\,s^{-1}$. The line represents the prediction of the model with $\varepsilon_0 = 0.11$ and a normalized binding energy at saturation $Q_s/A = 0.018$. The normalization is made here with the energy per unit length of an unclustered edge dislocation in pure Al, A. Q_s is the upper limit (saturation value) of the binding energy of the respective dislocation to the Mg cluster and corresponds to an infinite ageing time t_a. The model captures the continuously decreasing trend of the parameter with strain. As discussed in [19], increasing ε_0 leads to m_t moving in the vicinity of zero for all strains. Decreasing the rate causes m_t to become more negative and then to return in the vicinity of zero. Since the instantaneous rate sensitivity is positive, the steady state value is negative only at intermediate values of ε_0.

Fig. 11 shows the comparison of the model and experimental data for the variation of m_t with the temperature. The experimental results (open symbols and dashed line) are those from Fig. 3. The abscissa is the inverse temperature, $1/T$, which allows a direct comparison with $\log \varepsilon_0$. Note that since $\varepsilon_0 \propto \dot{\varepsilon}\ \exp[E/kT]$, $\log \varepsilon_0$ varies linearly with $1/T$. As seen in the figure, the model captures the general shape of the curve, with a minimum at intermediate values of ε_0. The fit is very good in the large ε_0 range, while in the low ε_0 range it is only approximate. The minima of the two curves were aligned by selecting the appropriate range of ε_0. This, however, does not change the overall shape of the curve. As in the case of the comparison in Fig. 10, the normalized binding energy Q_s/A was considered 0.018.

As discussed in [19], the shape of the m_t versus $\log \varepsilon_0$ curve changes with Q_s. As Q_s decreases, the curve in Fig. 11 retains its shape while the absolute value of m_t decreases. When Q_s tends to zero, which corresponds to high temperatures or/and low average solute concentrations, m_t vanishes.

It is interesting to compare the activation energies for PLC obtained from the slopes of the low and high temperature boundaries of the domain in Fig. 4, with the activation energies predicted by the model. In [19], the boundary of the negative SRS domain is described in terms of three exponential functions of the form:

$$\dot{\varepsilon}_{c1} \propto \exp\left[\frac{-E_{a1} + 1.6E_{a2}}{kT}\right] \tag{2a}$$

$$\dot{\varepsilon}_{c2} \propto \exp\left[\frac{-E_{a1} + 2.5E_{a2}}{kT}\right], \quad \text{and}$$

$$\dot{\varepsilon}_{c3} \propto \exp\left[\frac{-E_{a1} - 1.9E_{a2}}{kT}\right] \tag{2b}$$

The first function (2a) describes the high ε_0 boundary at all Q_s/A values, while the last two functions represent the low ε_0 boundary at high and low Q_s/A values, respectively (low/high

temperature or high/low average solute concentration). Since in the present case $Q_s/A = 0.018$, the relevant functions are the upper bound (2a) and the second of the two functions (2b).

In the $\log\dot{\varepsilon} - 1/T$ plane (Fig. 4), these are straight lines of slopes $-E_{a1} + 1.6E_{a2}$, and $-E_{a1} - 1.9E_{a2}$, respectively. E_{a1} is the activation energy for Mg diffusion in the bulk (controlling the rate of solute clustering at forests), and E_{a2} is an activation energy associated with the dissolution of clusters at large temperatures (controlling the saturation value of the binding energy, Q_s). The activation energy for bulk (vacancy-assisted) solute diffusion is 1.2 eV as measured by Fujikawa and Takada [45], and confirmed by atomistic simulations by Picu and Zhang [17]. An upper limit for the activation energy E_{a2} is provided by the largest binding energy of a Mg atom to the core of the forest dislocation. This quantity was evaluated by atomistic simulations and is 0.126, 0.092 and 0.043 eV for the binding of a single Mg atom to the core of edge, 60° and screw dislocations, respectively [46]. Considering E_{a1} = 1.2 eV and E_{a2} = 0.1 eV, the slope of the two boundaries correspond to 1.39 and 1.04 eV, which overestimates the values measured from Fig. 4 (1.09 and 0.86 eV).

Finally, the concept that clustering at forest dislocations leads to an increase of the strength of junctions formed with mobile dislocations and therefore of the athermal component of the flow stress, provides a justification for the variation of the yield/flow stress with temperature. This variation is shown in Fig. 8. At very low temperatures, below −100 °C, bulk diffusion is too sluggish and forest dislocations formed during deformation are not clustered. The fact that forests existing in the material before deformation are clustered is irrelevant, since the new forest dislocations control the rate of strain hardening. Hence, the variation with temperature of the athermal component of the flow stress is similar to that expected if the solute were immobile, and qualitatively similar to that in pure Al. A similar situation exists at temperatures above that at which forest clusters dissolve. In the intermediate range of temperatures, cluster formation at forests increases the strength of junctions, which leads to an increase in the athermal component of the flow stress. The thermally activated component of the flow stress is assumed to be unaffected by the presence of clusters. This behavior is shown schematically in Fig. 12. For clarity, the effect of recovery was neglected such that, at given strain, the athermal component of the flow stress is temperature independent in absence of solute clusters. The total flow stress results as the sum of the two curves in the figure, which leads to the plateau in Fig. 8. The plateau may be flat, rising or slightly decreasing with temperature, depending on the relative magnitude of the components shown in Fig. 12.

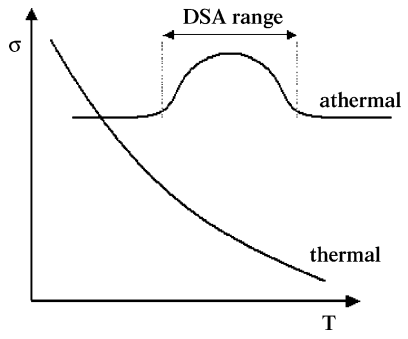

Fig. 12. Schematic representation of the variation with temperature of the thermally activated and athermal components of the flow stress. The effect of dynamic recovery that would affect the athermal component (imposing a generally decreasing trend with increasing T) is neglected, for clarity. The increase of the athermal component in the DSA range is due to the increase of the strength of dislocation junctions induced by solute clustering at forest dislocations.

6. Conclusion

The mechanical behavior of the commercial Al alloy AA5182-O in as-received conditions is studied. The PLC effect is observed at all temperatures between −80 and 110 °C and at strain rates lower than $10^{-1}\,s^{-1}$. The experimental observations are compared with the predictions of a model based on the observation that solute clusters formed at forest dislocations lead to an increase of the strength of dislocations junctions, or the athermal component of the flow stress. The model captures many of the macroscopically observed features of the negative SRS and offers a new explanation for the observed anomalous variation of the flow stress (at given strain) and hardening rate with temperature in the negative SRS domain.

Acknowledgment

This work was supported, in part, by the Alcoa Inc. and by the NSF through grant CMS-0084987. JJG, FB and GV are indebted to the Portuguese Foundation of Science and Technology (FCT) and program POCTI/CTM/42724/2001 for financial support.

References

[1] A. van den Beukel, Phys. Stat. Sol. A 30 (1975) 197.
[2] R.A. Mulford, U.F. Kocks, Acta Metall. 27 (1979) 1125.
[3] P.G. Mccormick, Y. Estrin, Scripta Met. 23 (1989) 1231.
[4] L.P. Kubin, Y. Estrin, Acta Met. Mater. 38 (1990) 697.
[5] E.O. Hall, Yield Point Phenomena in Metals and Alloys, Macmillan, London, 1970.
[6] J. Balik, P. Lukac, Acta Met. Mater. 41 (1993) 1447.
[7] H. Fujita, T. Tabata, Acta Met. 25 (1977) 793.
[8] T. Tabata, H. Fujita, Y. Nakajima, Acta Met. 28 (1985) 795.
[9] A.T. Thomas, Acta Met. 14 (1966) 1363.
[10] C.P. Hinesly, J.G. Morris, Mater. Sci. Eng. 6 (1970) 48.
[11] D.J. Lloyd, Metall. Trans. A 11 (1980) 1287.
[12] A. Korbel, H. Dybiec, Acta Met. 29 (1981) 89.
[13] M. Li, D.J. Lege, J. Eng. Mater. Technol. 48 (1998) 120.
[14] J.M. Robinson, M.P. Shaw, Int. Mater. Rev. 39 (1994) 113.
[15] J.M. Robinson, Int. Mater. Rev. 39 (1994) 217.

[16] A.W. Sleeswyk, Acta Met. 6 (1958) 598.
[17] R.C. Picu, D. Zhang, Acta Mater. 52 (2004) 161.
[18] L.J. Cuddy, W.C. Leslie, Acta Metall. 20 (1972) 1157.
[19] R.C. Picu, Acta Mater. 52 (2004) 3447.
[20] S.M. de la Puente, B. Verlinden, L. Delaey, J. Mater. Sci. 29 (1994) 6167.
[21] P. Ratchev, B. Verlinden, P. van Houtte, Acta Met. Mater. 43 (1995) 621.
[22] P. Ratchev, B. Verlinden, P. van Houtte, P. de Smet, Mater. Sci. Eng. A 222 (1997) 189.
[23] H. Weiland, J.M. Fridy, E. Llewellyn, Mater. Sci. Forum 408–412 (2002) 101.
[24] C.P. Ling, P.G. McCormick, Acta Met. Mater. 41 (1993) 3127.
[25] C.P. Ling, P.G. McCormick, Acta Met. Mater. 38 (1990) 2631.
[26] R.H. Wagoner, N.M. Wang, Metall. Trans. A 14 (1983) 2395.
[27] E. Pink, A. Grinberg, in: R.F. Grifkins (Ed.), Strength of Metals and Alloys, vol. 1, Pergamon, Oxford, 1982, p. 83.
[28] A. Nortmann, C. Schwink, Acta Mater. 45 (1997) 2043.
[29] A. Nortmann, C. Schwink, Acta Mater. 45 (1997) 2051.
[30] P. Hahner, Acta Mater. 45 (1997) 3695.
[31] M. Abbadi, P. Hahner, A. Zeghloul, Mater. Sci. Eng. A 337 (2002) 194.
[32] E. Pink, A. Grinberg, Acta Metall. 30 (1982) 2153.
[33] E. Pink, Acta Met. 37 (1989) 1773.
[34] R. Kral, P. Lukac, Mater. Sci. Eng. A 234–236 (1997) 786.
[35] E. Romhanji, M. Popovic, V. Radmilovic, Zeitsh. Metall. 90 (1999) 305.
[36] K. Chihab, Y. Estrin, L.P. Kubin, J. Vergnol, Scripta Met. 21 (1987) 203.
[37] W.M. Webernig, J. Krol, E. Pink, Mater. Sci. Eng. 80 (1986) 16.
[38] R. Hill, The Mathematical Theory of Plasticity, Clarendon Press, Oxford, 1950.
[39] S. Ohtani, H. Inagaki, Mater. Sci. Forum 396–402 (2002) 1049.
[40] R. Kral, P. Lukac, M. Janacek, Mater. Sci. Forum 217–222 (1996) 1025.
[41] D.J. Skinner, M.S. Zedalis, P. Gilman, Mater. Sci. Eng. A119 (1989) 81.
[42] D.J. Lloyd, K. Tangri, Mater. Sci. Eng. 10 (1972) 75.
[43] K. Hanson, J.W. Morris, J. Appl. Phys. 46 (1975) 2378.
[44] P. Wycliffe, U.F. Kocks, J.D. Embury, Scripta Metall. 14 (1980) 1349.
[45] S.-I. Fujikawa, Y. Takada, Defect Diff. Forum 143–147 (1997) 409.
[46] D. Zhang, R.C. Picu, Model. Simul. Mater. Sci. Eng. 12 (2004) 121.